

LOW-FIELD MAGNETIC RESONANCE IMAGING OF THE EQUINE TARSUS: NORMAL ANATOMY

MARGARET A. BLAIK, DVM, R. REID HANSON, DVM, STEVEN A. KINCAID, DVM, MS, PHD,
JOHN T. HATHCOCK, DVM, MS, JUDITH A. HUDSON, DVM, PHD, DEBRA K. BAIRD, DVM, PHD

The objective of this study was to define the normal gross anatomic appearance of the adult equine tarsus on a low-field magnetic resonance (MR) image. Six radiographically normal, adult, equine tarsal cadavers were utilized. Using a scanner with a 0.064 Tesla magnet, images were acquired in the sagittal, transverse and dorsal planes for T1-weighted and the sagittal plane for T2-weighted imaging sequences. Anatomic structures on the MR images were identified and compared with cryosections of the imaged limbs. Optimal image planes were identified for the evaluation of articular cartilage, subchondral bone, flexor and extensor tendons, tarsal ligaments, and synovial structures. MR images provide a thorough evaluation of the anatomic relationships of the structures of the equine tarsus. *Veterinary Radiology & Ultrasound*, Vol. 41, No. 2, 2000, pp 131-141.

Key words: low-field magnetic resonance imaging, equine, horse, tarsus, hock, anatomy.

Introduction

LAMENESS LOCALIZED TO the tarsus has been reported to account for up to 80% of chronic, low grade hindlimb lameness in horses.¹ The complex anatomy of the tarsus, with its multiple small bones and numerous synovial and soft tissue structures, is predisposed to numerous pathologic processes. The majority of tarsal lameness in the horse results from osteoarthritis, osteochondrosis, traumatic fractures, tendon and ligament damage, and synovial disease. Both articular cartilage damage (osteoarthritis, osteochondrosis, and articular fractures), subchondral bone damage, and soft tissue injury (tendinitis and desmitis) play important roles in tarsal lameness.

Magnetic resonance (MR) imaging has been successful in humans for the diagnosis of musculoskeletal disease.⁶ MR imaging is the only non-invasive modality that allows direct evaluation of articular cartilage, subchondral bone and soft tissue structures surrounding joints. Previous studies describing MR imaging of equine limbs are evidence of the potential of this modality for early detection of cartilage and subchondral bone lesions associated with degenerative joint disease, and with soft tissue injury associated with tendon

and ligamentous lesions.^{2,3} Early visualization of cartilage defects will help in the determination of prognosis and the clinical benefit of treatment.

Advantages of MR imaging include multiplanar imaging capabilities, superior contrast resolution of soft tissue structures, and the absence of ionizing radiation.⁴ In addition, MR imaging allows assessment of physiologic differences between normal and abnormal tissues by utilization of various imaging sequences.

We examined the anatomy of the adult equine tarsus using MR imaging in transverse, sagittal and dorsal planes, with T1- and T2-weighted imaging sequences. The optimal imaging planes for articular cartilage, osseous structures, and peri-articular soft tissue structures of the tarsus were determined.

Materials and Methods

Six cadaver hindlimbs from three mature horses (3-year-old thoroughbred mare, 3-year-old thoroughbred gelding, 10-year-old Tennessee Walking Horse gelding) were studied. The limbs were obtained from horses donated to the Auburn University College of Veterinary Medicine Large Animal Clinic that died or were euthanized due to an untreatable disease unrelated to any musculoskeletal disorder of the hindlimbs. Tarsi of each horse were radiographed prior to harvesting to ensure that no radiographic abnormalities were present. Limbs were removed by disarticulating at the stifle joint, and shoes and nails, if present, were removed. Mineral oil-filled plastic capsules were attached to each limb as reference points for sectioning and comparison of images with anatomic sections.

Limbs were scanned within 2 hours after euthanasia.

From the Department of Radiology (Blaik, Hathcock, Hudson), Department of Large Animal Surgery and Medicine (Hanson), and the Department of Anatomy, Physiology, and Pharmacology (Baird, Kincaid), Auburn University, Auburn, AL.

Address correspondence and reprint requests to Margaret A. Blaik, DVM, Department of Radiology, Auburn University, Auburn, AL 36849-5522.

Received May 11, 1999; accepted for publication July 30, 1999.

Supported by a grant from Auburn University Research Grant and Aid No 94-065, Auburn University, AL.

TABLE 1. Parameters of MR Imaging Equipment for Acquiring T1-Weighted Transverse, Sagittal, Dorsal and T2-Weighted Sagittal Images of the Adult Equine Tarsus.

Parameter	T1 Weighted Transverse	T1-Weighted Sagittal	T1-Weighted Dorsal	T2-Weighted Sagittal
TR (msec)	68	68	68	145
TE (msec)	24	24	24	53
Slice Thickness (mm)	4.5	3.5	4.5	3.5
Flip Angle (°)	45	90	45	16, 20
Matrix Size	256 × 252	256 × 252	252 × 256	252 × 256
Field of View (cm)	18.0 × 18.0	18.0 × 18.0	18.0 × 18.0	28.0 × 28.0
Number of Excitations	1	2	2	2
Imaging Time (min:sec)	9:29	18:59	18:59	20:15
Resolution (mm pixel)	0.7 × 0.7	0.7 × 0.7	0.7 × 0.7	1.10 × 1.10

Each joint was placed in an extended position within a solenoidal human extremity coil and imaged with a 0.064 Tesla magnet.* The imaging protocol consisted of a sagittal locator image, followed by three dimensional Fourier transform (3DFT) T1-weighted transverse plane gradient echo

images, dorsal plane 3DFT gradient echo images, sagittal plane 3DFT T1-weighted gradient echo images, and sagittal plane 2DFT T2-weighted images (Table 1).

After imaging, the limbs were frozen at -18 °C in the same position as they had been imaged with the mineral oil capsule markers still in place. The limbs were then sliced into 4 mm sections corresponding to one of the three MR image planes (three dorsal, two transverse and one sagittal). Each section was photographed for comparison to its cor-

*Access, Toshiba America MRI, San Francisco, CA.

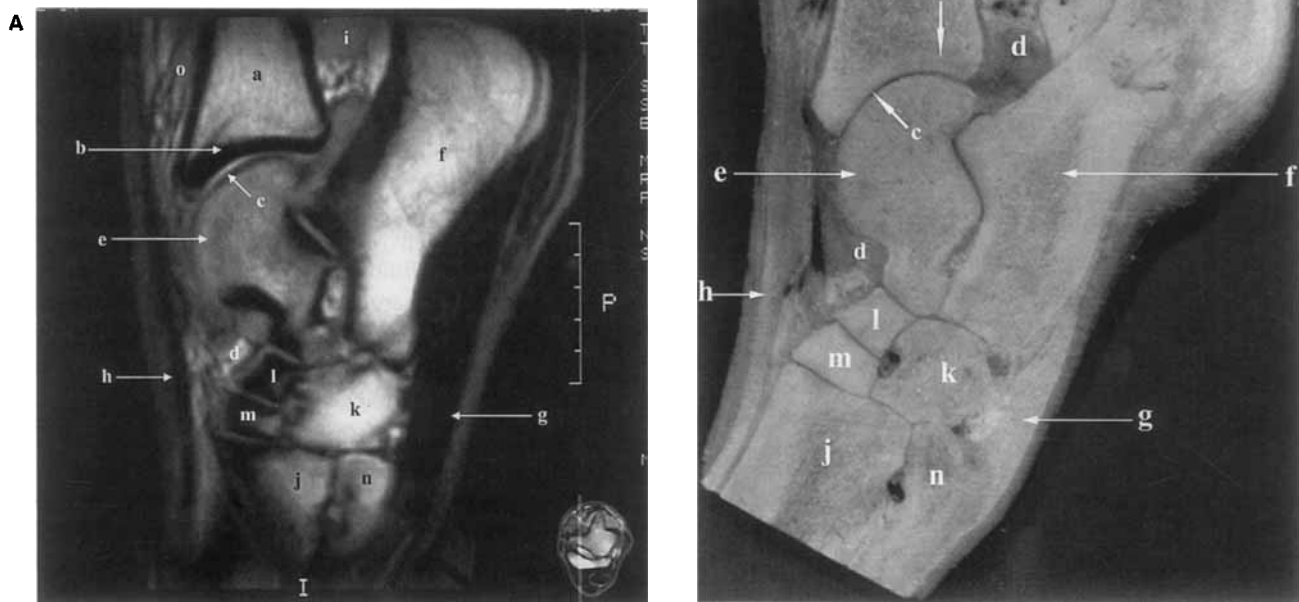


FIG. 1. (A) Lateral sagittal plane T1-weighted image and (B) gross anatomic section at the level of the lateral trochlea of the talus. a) marrow of tibia; b) subchondral bone of tibia; c) articular cartilage of tarsocrural joint; d) synovium of tarsocrural joint; e) lateral ridge of trochlea tali; f) calcaneus; g) long plantar ligament; h) tendon of long digital extensor; i) deep digital flexor muscle; j) metatarsal III; k) fourth tarsal bone; l) central tarsal bone; m) third tarsal bone; n) metatarsal IV; o) tibialis cranialis muscle; p) tendon of peroneus tertius muscle; q) common calcaneal tendon.

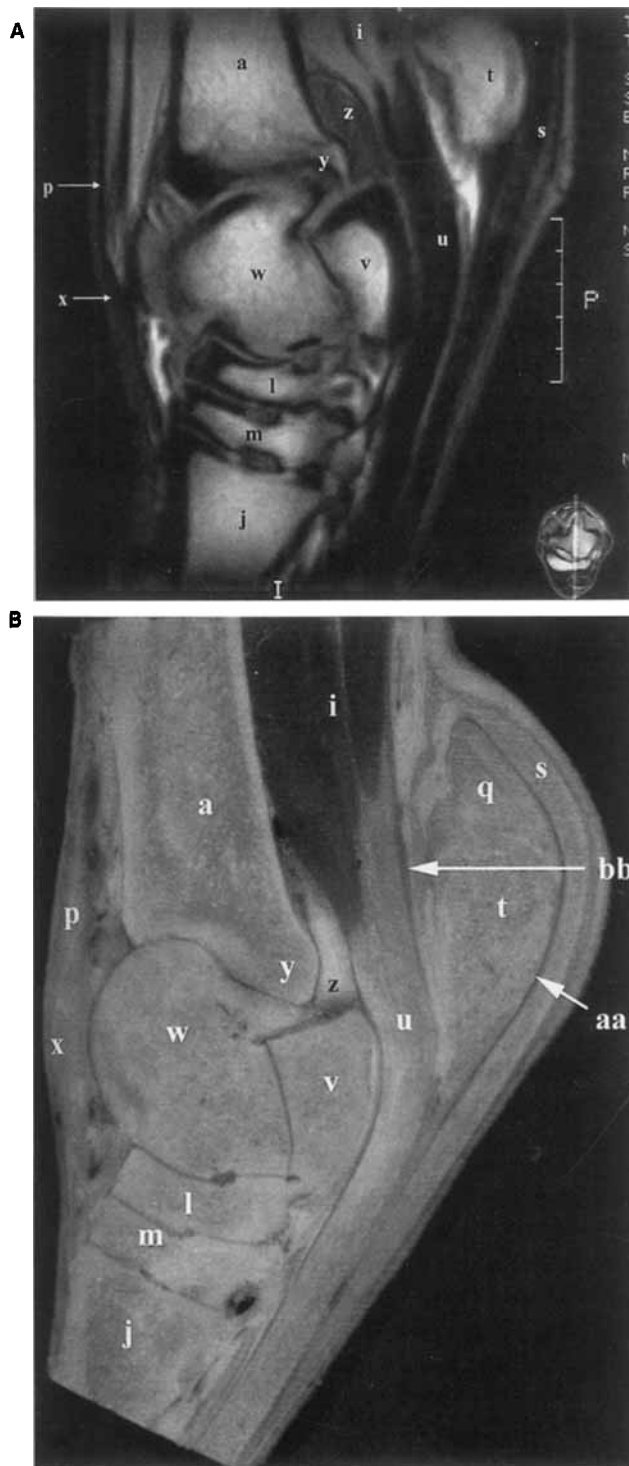


FIG. 2. (A) Mid-sagittal plane T1-weighted MR image and (B) gross anatomic section. a) marrow of the tibia; i) deep digital flexor muscle; j) metatarsal III; l) central tarsal bone; m) third tarsal bone; p) tendon of the peroneus tertius muscle; q) common calcanean tendon; s) tendon of superficial digital flexor; t) tuber calcanei; u) tendon of deep digital flexor; v) sustentaculum tali; w) talus; x) medial tendon of tibialis cranialis muscle (cunean tendon); y) caudal aspect of intermediate ridge of tibial cochlea; z) tarsocrural synovium; aa) calcanean bursa; bb) tendon sheath of deep digital flexor (tarsal sheath).

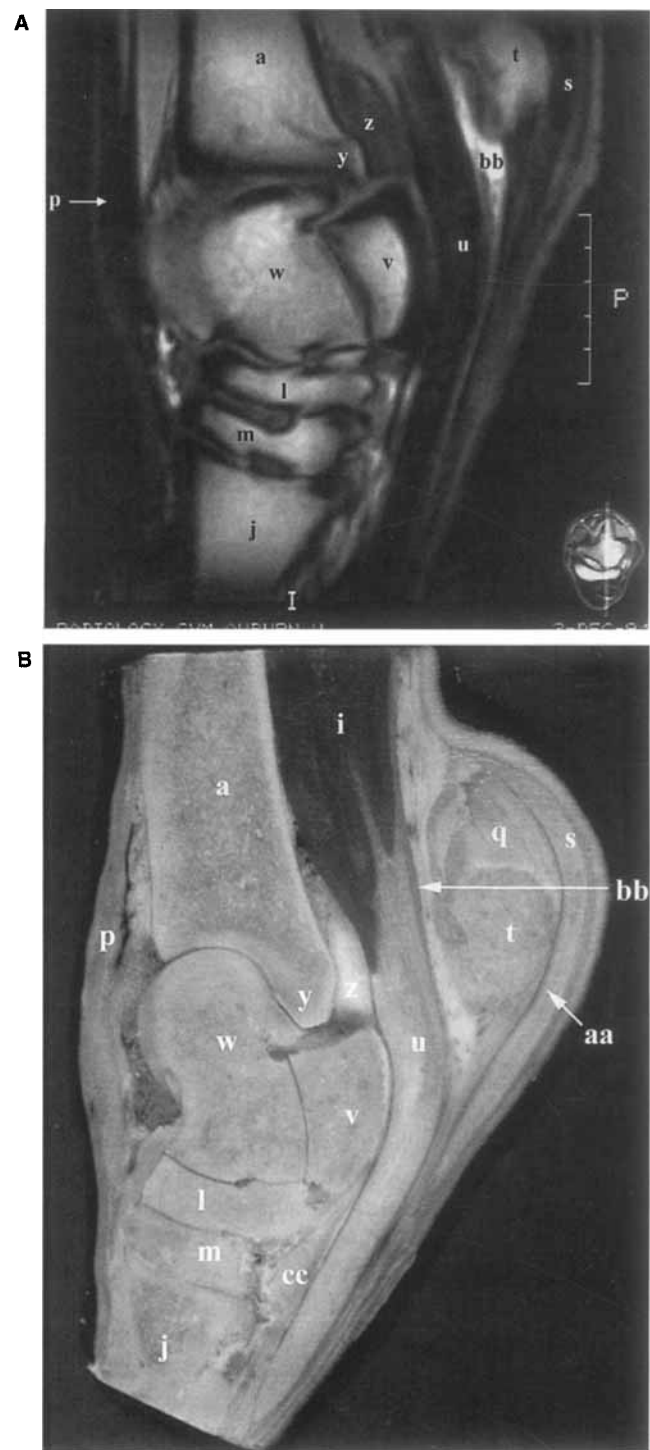


FIG. 3. (A) Medial sagittal plane T1-weighted MR image and (B) gross anatomic section at the level of the medial trochlea of the talus. a) marrow of tibia; i) deep digital flexor muscle; j) metatarsal III; l) central tarsal bone; m) third tarsal bone; p) tendon of peroneus tertius muscle; q) common calcanean tendon; s) tendon of superficial digital flexor; t) tuber calcanei; u) tendon of deep digital flexor; v) sustentaculum tali; w) talus; z) tarsocrural synovium; aa) calcanean bursa; bb) tendon sheath of deep digital flexor (tarsal sheath); cc) fused first and second tarsal bone.

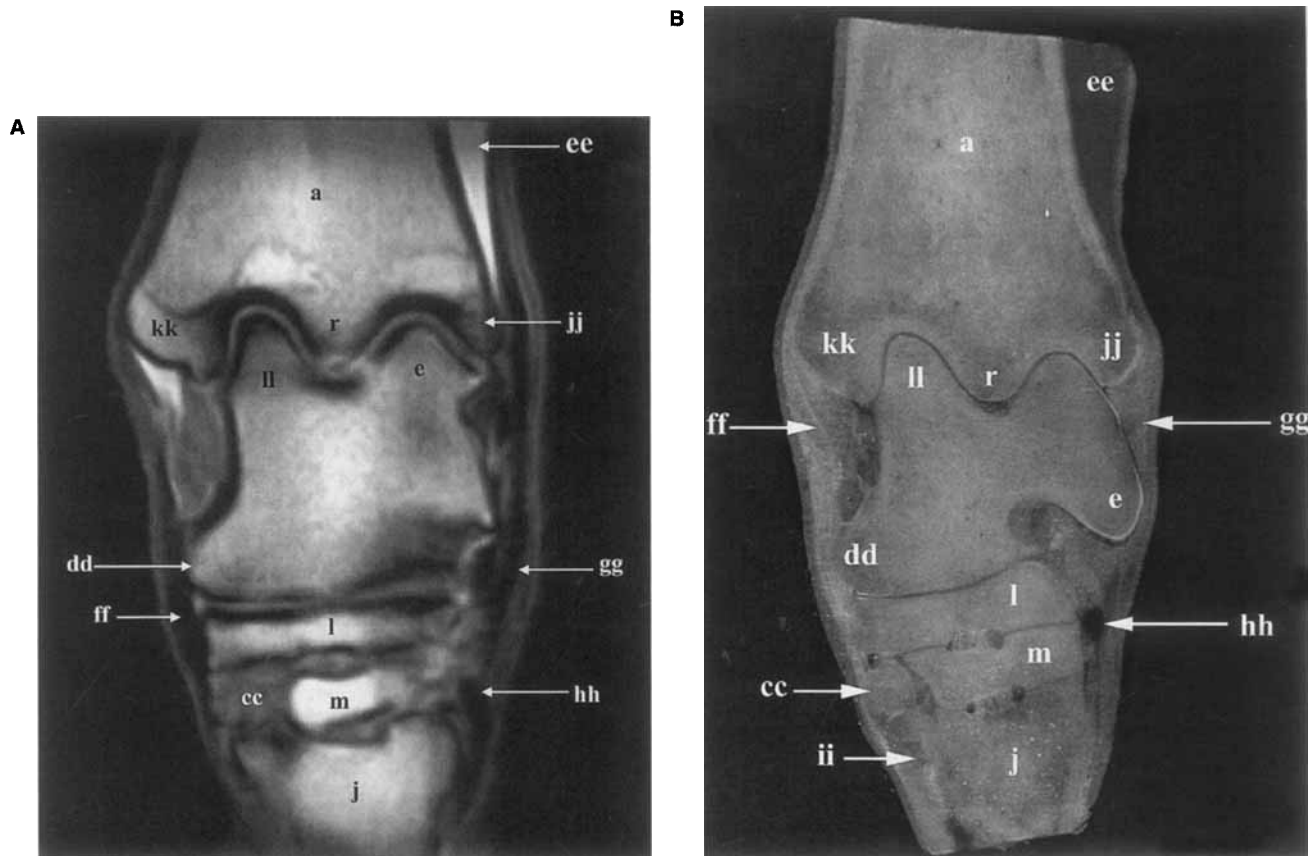


FIG. 4. (A) Cranial dorsal plane T1-weighted MR image and (B) gross anatomic section. a) marrow of tibia; e) lateral ridge of trochlea tali; j) metatarsals III; l) central tarsal bone; m) third tarsal bone; r) cranial aspect of intermediate ridge of tibial cochlea; cc) fused first and second tarsal bones; dd) distal tubercle of talus; ee) lateral digital extensor muscle; ff) medial collateral ligaments of tarsus; gg) lateral collateral ligaments of tarsus; hh) dorsal metatarsal artery III; ii) metatarsal IV; jj) lateral malleolus of tibia; kk) medial malleolus of tibia; ll) medial ridge of trochlea tali.

responding MR image for confirmation of anatomic structures.

Results

The findings of this study are formatted as sequential pairs of a MR image and its corresponding gross anatomic section. Anatomy texts were consulted for the identification and confirmation of various anatomic structures.⁵⁻⁸ Sagittal, dorsal, and transverse T1-weighted images and sagittal T2-weighted images are shown. T1-weighted sagittal plane images begin laterally (Figs. 1-3), dorsal plane images begin craniodorsally (Figs. 4 and 5), and transverse images begin proximally (Figs. 6-9). T2-weighted images are shown in the sagittal plane and also begin laterally (Figs. 10 and 11).

In the T1 images, fat and trabecular bone (presumably due to fat content within the bone marrow) had a bright or white indicating high signal intensity. Cortical and subchondral bone had a black due to low signal intensity, which allowed for clear differentiation between subchondral or cortical bone from trabecular bone. Tendon and ligaments had low signal and appeared dark gray to black. Muscle was of intermediate signal intensity and appeared in various

shades of gray. Articular cartilage appeared as a single layer of homogenous intermediate to high signal intensity adjacent to the low signal of subchondral bone at articular interfaces. Synovial tissue and synovial fluid appeared dark gray. T1 weighted images provide excellent anatomic detail of the peri-articular structures.

In the T2 weighted images, the synovium was of high signal intensity, whereas cartilage and subchondral bone appeared dark due to low signal intensity. The cartilage-bone interface on the T2 weighted images was difficult to establish. Trabecular bone was of intermediate signal intensity, and the tendinous and ligamentous structures were of low signal intensity. The T2 images allowed better visualization of the synovium; however, the detail of the images was not as clear as in T1-weighted images. Table 2 lists the characteristic appearance of various normal tissues on T1 and T2-weighted MR images.

Bones/Joints

All T1-weighted imaging planes provided useful information for evaluation of osseous structures. The sagittal and dorsal planes allowed evaluation of articular alignment,

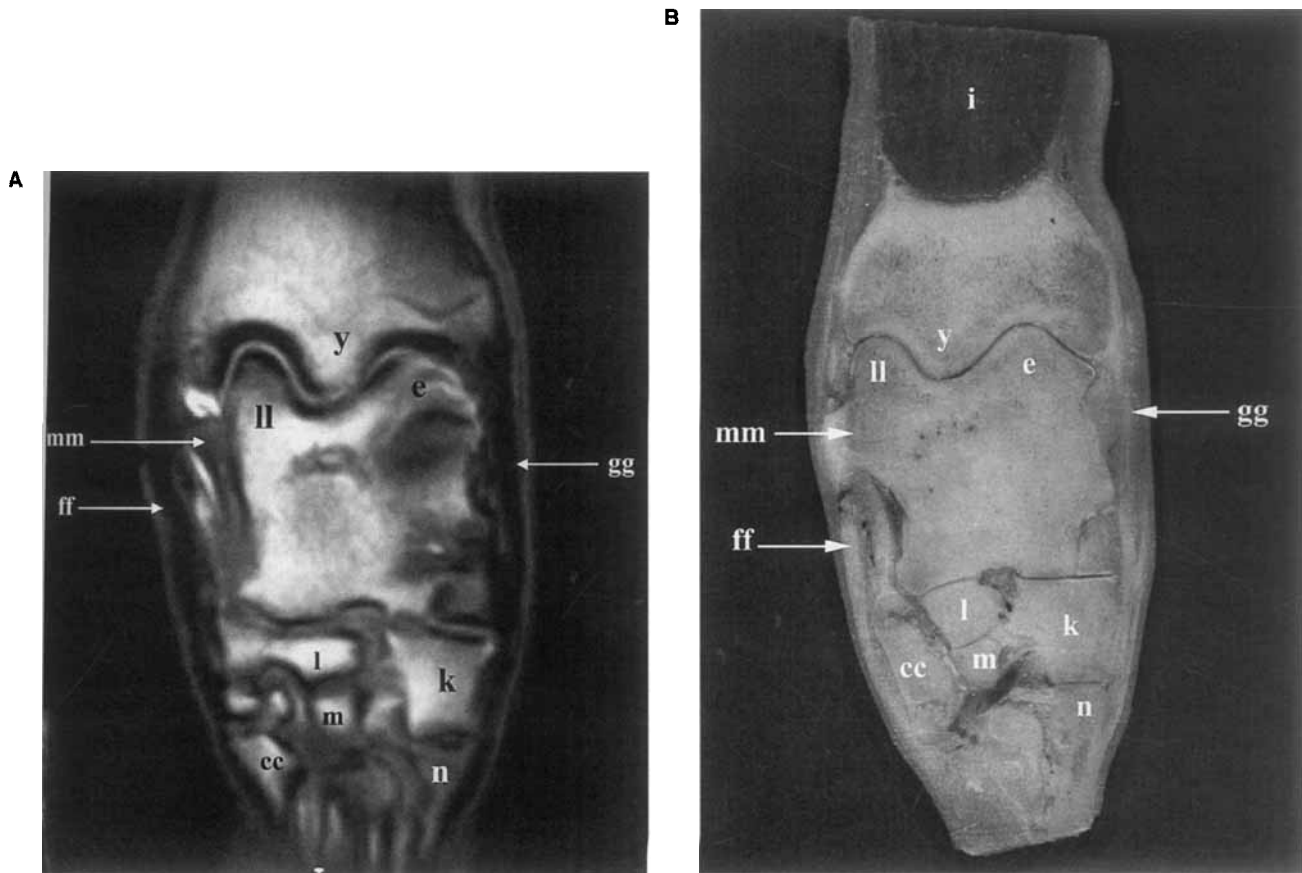


FIG. 5. (A) Caudal dorsal plane T1-weighted MR image and (B) gross anatomic section. e) lateral ridge of trochlea tali; i) deep digital flexor muscle; k) fourth tarsal bone; l) central tarsal bone; m) third tarsal bone; n) metatarsal IV; y) caudal aspect of intermediate ridge of tibial cochlea; cc) fused first and second tarsal bones; ff) medial collateral ligaments of tarsus; gg) lateral collateral ligaments of tarsus; mm) proximal tuberosity of talus; ll) medial ridge of trochlea tali.

while the transverse plane provided the most detailed evaluation, especially of the smaller tarsal bones. Specific sites of interest were more clearly defined in certain planes. The trochlear ridges of the talus were well visualized in all three planes (Figs. 1–9). The contour of these ridges and the articular cartilage of the non-weight bearing aspect were most evident in the sagittal images (Figs. 1–3); however, because of the obliquity of these ridges, it was not possible to follow a continuous line of articular cartilage along them in a single sagittal plane. In dorsal and transverse planes, articular cartilage of the trochlear ridges was more clearly delineated (Figs. 4–9). The articular cartilage surface of the distal tibia had a similar appearance and could be visualized in all three planes. Other important osseous landmarks, including both the lateral and medial malleoli of the tibia and the proximal and distal tuberosities of the talus, were better visualized in the dorsal plane images (Figs. 4 and 5). The sustentaculum tali of the calcaneus was best imaged in the transverse plane (Figs. 6–9). Its relationship to the tarsal sheath was best evaluated in cross section. The transverse plane provided the most complete visualization of the multiple small intertarsal articulations, and allowed assessment

of the integrity of the small tarsal bones (Figs. 6–9); however, care must be taken to assess the level of the section.

The synovium was best visualized in the T2-weighted images (Figs. 10 and 11). It appeared as a bright white signal within articular spaces and surrounding tendons within the sheathed portions. The plantar portion of the tarsocrural joint capsule was well visualized in the sagittal planes of the T1-weighted images as an area of mixed signal intensities with both intermediate and low signals produced.

Tendons and Ligaments

The transverse and sagittal planes were best for evaluation of the tendinous and ligamentous structures surrounding the equine tarsus (Figs. 1–3, 6–9). The linear fiber pattern of these structures was seen best in the sagittal plane. In the transverse plane, flexor and extensor tendons, their associated sheaths, and their relationships to osseous structures were well recognized. In T1 and T2-weighted images, tendons and ligaments had low signal intensity and appeared dark. A mixed signal is present in the deep digital flexor tendon in the more proximal transverse images (Figs.

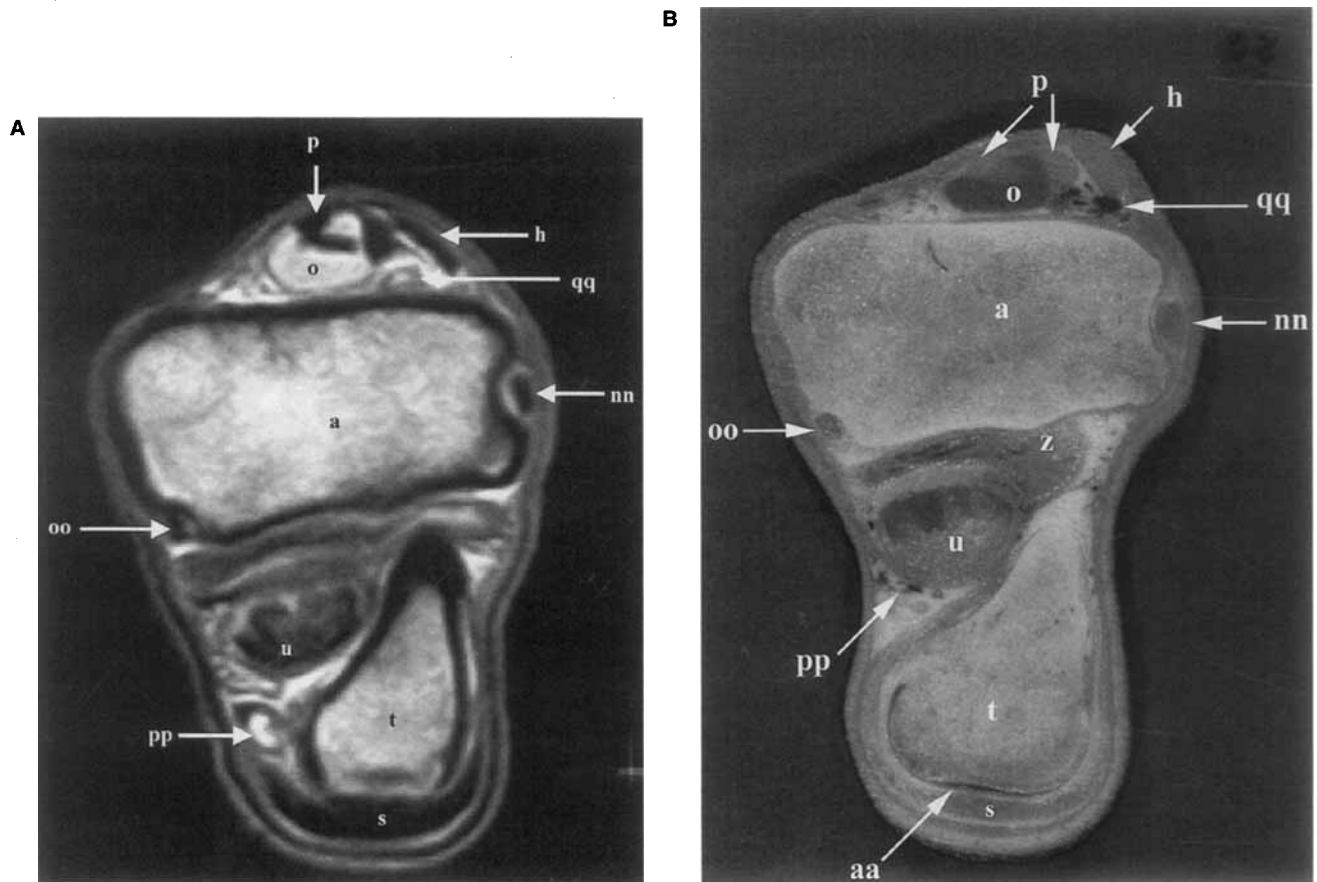


FIG. 6. (A) Transverse plane T1-weighted MR image and (B) gross anatomic section at the level of the distal tibia. a) marrow of tibia; h) tendon of the long digital extensor; o) tibialis cranialis muscle; p) tendon of the peroneus tertius muscle; s) tendon of superficial digital flexor; t) tuber calcanei; u) tendon of deep digital flexor; z) tarsocrural synovium; aa) calcaneal bursa; nn) tendon of lateral digital extensor muscle; oo) tendon of medial head of deep digital flexor; pp) tibial nerve and saphenous vein; qq) deep peroneal nerve and cranial tibial vessels.

6,7). This most likely represents the presence of muscle fibers in these proximal sections. The T1 images provided the best resolution for anatomic structures; however, contrast between the very high signal intensity of synovial sheaths and low signal intensity of tendons provided by T2 weighted images made it easier to define boundaries.

Specific tendinous and ligamentous structures were best defined in different planes. The superficial digital flexor tendon was well visualized in transverse and sagittal plane T1-weighted images as a linear band of low signal intensity coursing along the plantar aspect of the limb. However, it was not identified in the dorsal images we obtained. Transverse plane T1-weighted images provided the most complete evaluation of the deep digital flexor tendon (DDFT) and its associated tarsal sheath as it passed over the plantaromedial aspect of the limb (Figs. 6–9). The anatomic location of the tendon was evident in both the sagittal and transverse plane images where the tendon was identified crossing the sustentaculum tali (Figs. 2 and 7). The sagittal T1-weighted images also allowed adequate visualization, and the sagittal T2-weighted images provided excellent con-

trast between the DDFT and the synovial fluid and tissues of the tarsal sheath (Fig. 10). The, long and lateral digital extensor tendons were most clearly evaluated in the transverse plane T1-weighted images as round to oval low signal intensity structures that passed over the dorsal and lateral aspects of the tarsus, respectively (Figs. 6–9). The sagittal and dorsal T1-weighted views provided less than optimal viewing of these structures. The medial tendon of the tibialis cranialis muscle (cunean tendon) was seen in cross section on the mid-sagittal T1 image as an oval structure of low signal intensity situated on the dorsal aspect of the tarsus (Fig. 2). This tendon was not clearly visualized.

Ligamentous structures of importance include the medial and lateral collateral ligaments and the long plantar ligament. Collateral ligaments are separated into short and long divisions; however, these separations were not evident (other than known origin and insertion points) on the MR or gross images. Collateral ligaments were best evaluated in the T1-weighted transverse plane images; however, they were incompletely visualized in the T1-weighted dorsal plane images and not visualized at all in the T1-weighted

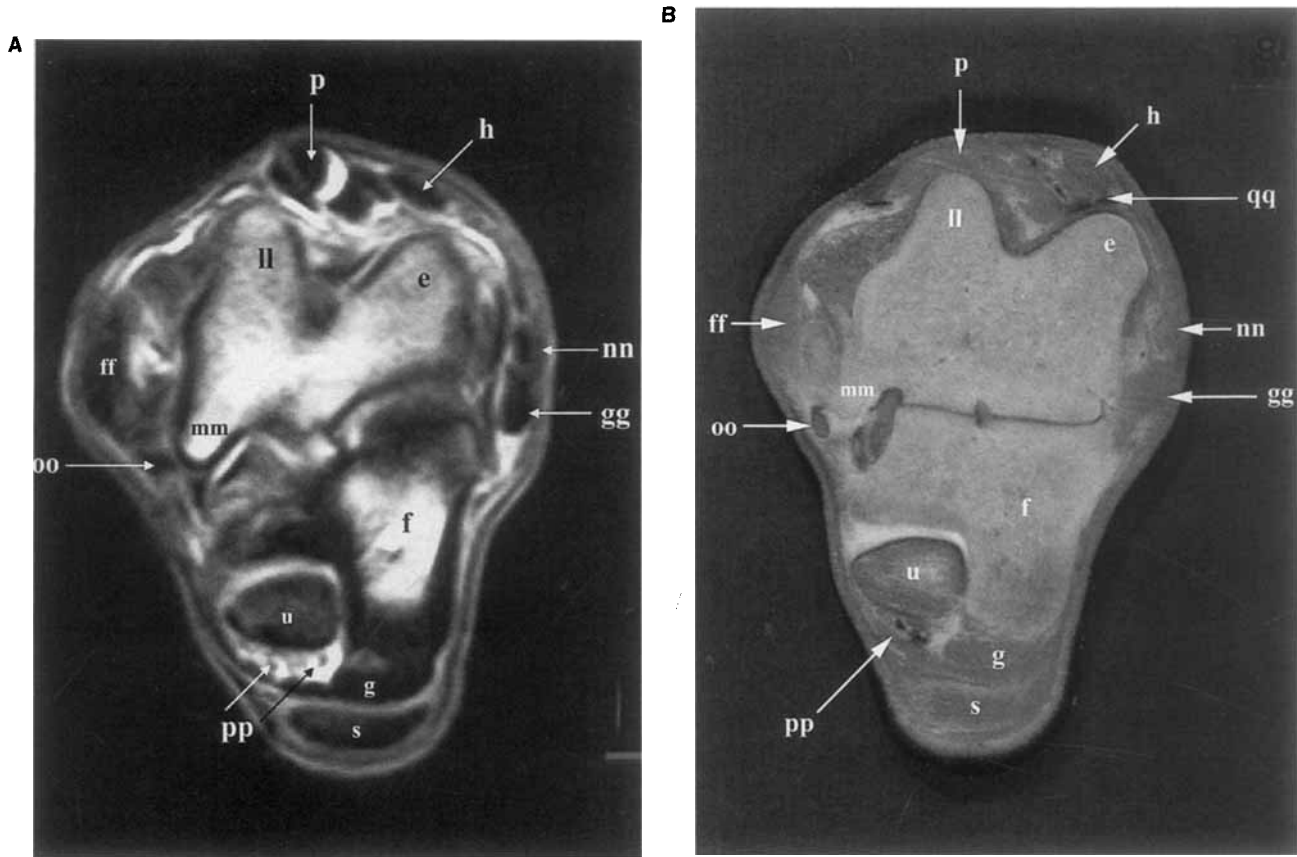


FIG. 7. (A) Transverse plane T1-weighted MR image and (B) gross anatomic section at the level of the trochlear ridges of the talus. e) lateral ridge of trochlea tali; f) calcaneus; g) long plantar ligament; h) tendon of the long digital extensor; p) tendon of peroneus tertius muscle; s) tendon of superficial digital flexor; u) tendon of deep digital flexor, ff) medial collateral ligaments of tarsus; gg) lateral collateral ligaments of tarsus; ll) medial ridge of trochlea tali; mm) proximal tuberosity of talus; nn) tendon of lateral digital extensor muscle; oo) tendon of medial head of deep digital flexor; pp) tibial nerve and saphenous vessels; qq) deep peroneal nerve and cranial tibial vessels.

sagittal images (Figs. 6–9). The long plantar ligament (LPL) was most thoroughly evaluated in the T1-weighted transverse plane as a rounded structure of low signal intensity that originated on the plantar aspect of the calcaneus and continued distally to the proximal fourth metatarsal bone (Figs. 6–9). The T1-weighted sagittal plane was useful for assessing the relationship between the LPL and calcaneus (Fig. 2). The long plantar ligament was not included in the T1-weighted dorsal plane images.

Neurovascular Structures

Several neurovascular structures were visualized in the MR images. The saphenous vessels and cranial tibial vessels were best seen in transverse plane images as small, focal, circular, white areas of high signal intensity in both T1 and T2 images that were plantar to the DDFT and just dorsal to the trochlear ridges of the talus, respectively (Figs. 6–8). Dorsal metatarsal artery III was imaged in the dorsal plane as a discrete circular focus of high signal intensity located just lateral to the distal intertarsal joint (Fig. 5). The respective nerves, could not be differentiated as distinct structures from the vessels.

Discussion

The equine tarsus is well suited for magnetic resonance imaging. Its narrow linear profile and minimal soft tissue coverage allows for the close placement of surface radio-frequency receiver coils. In this study, a 0.064 Tesla magnet was used to obtain T1 and T2-weighted magnetic resonance images of cadaver tarsi. Our goal was to obtain good quality images of the peri-articular soft tissue structures and articular surfaces for comparison with gross anatomic sections. This required adequate signal-to-noise ratio and contrast. Imaging time, although not a primary factor, was recorded since horses undergoing MRI at our institution will be under general anesthesia and timely imaging would be preferred.

The continuum of signal intensities seen in this study are similar to those previously reported for low-field MR imaging in both animals and humans.^{9–11} The T1-weighted images provided the greatest anatomic detail, most likely because of improved signal-to-noise ratio (SNR). Peri-articular tendinous and ligamentous structures were well defined in both the T1 and T2-weighted images, with the T2-weighted images providing excellent visualization of

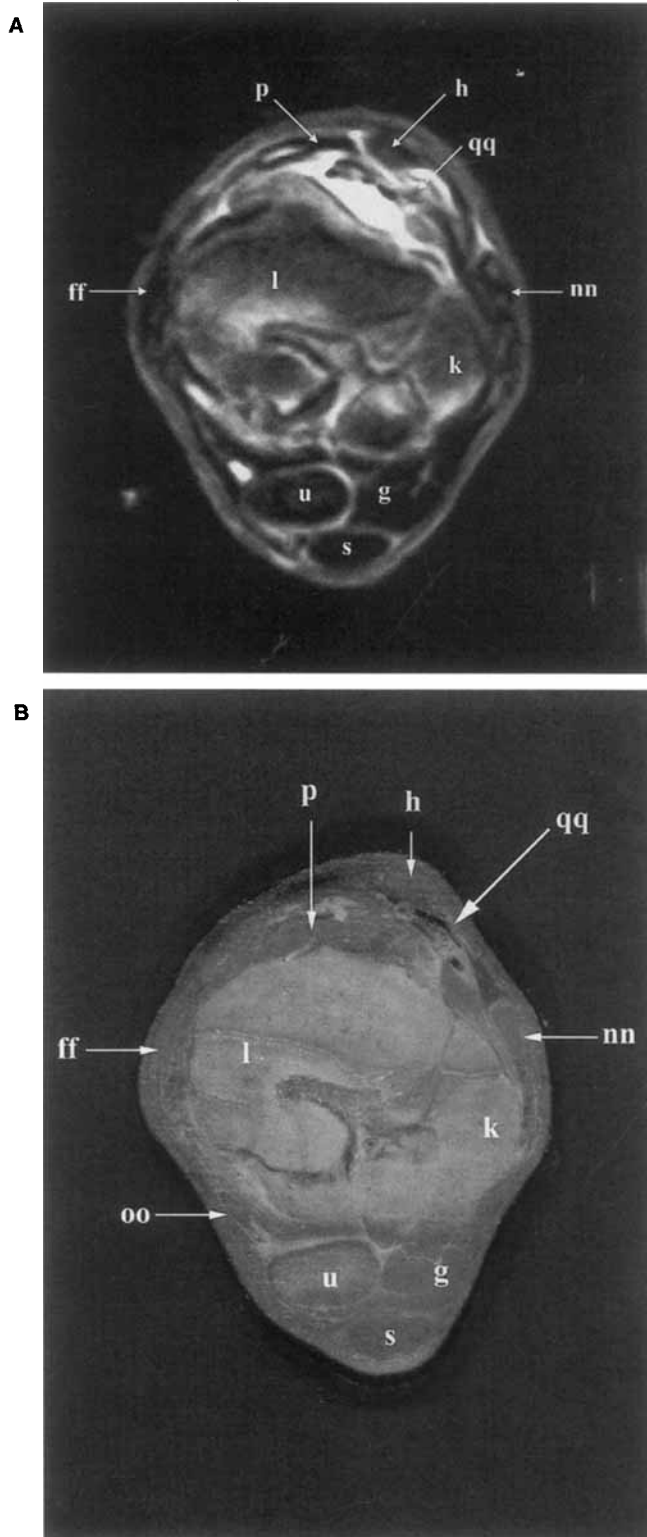


FIG. 8. (A) Transverse plane T1-weighted MR image and (B) gross anatomic section at the level of the proximal row of tarsal bones. g) long plantar ligament; h) tendon of the long digital extensor; k) fourth tarsal bone; l) central tarsal bone; p) tendon of the peroneus tertius muscle; s) tendon of superficial digital flexor; u) tendon of deep digital flexor; ff) medial collateral ligaments of tarsus; nn) tendon of lateral digital extensor; oo) tendon of medial head of deep digital flexor; qq) deep peroneal nerve and cranial tibial vessels.

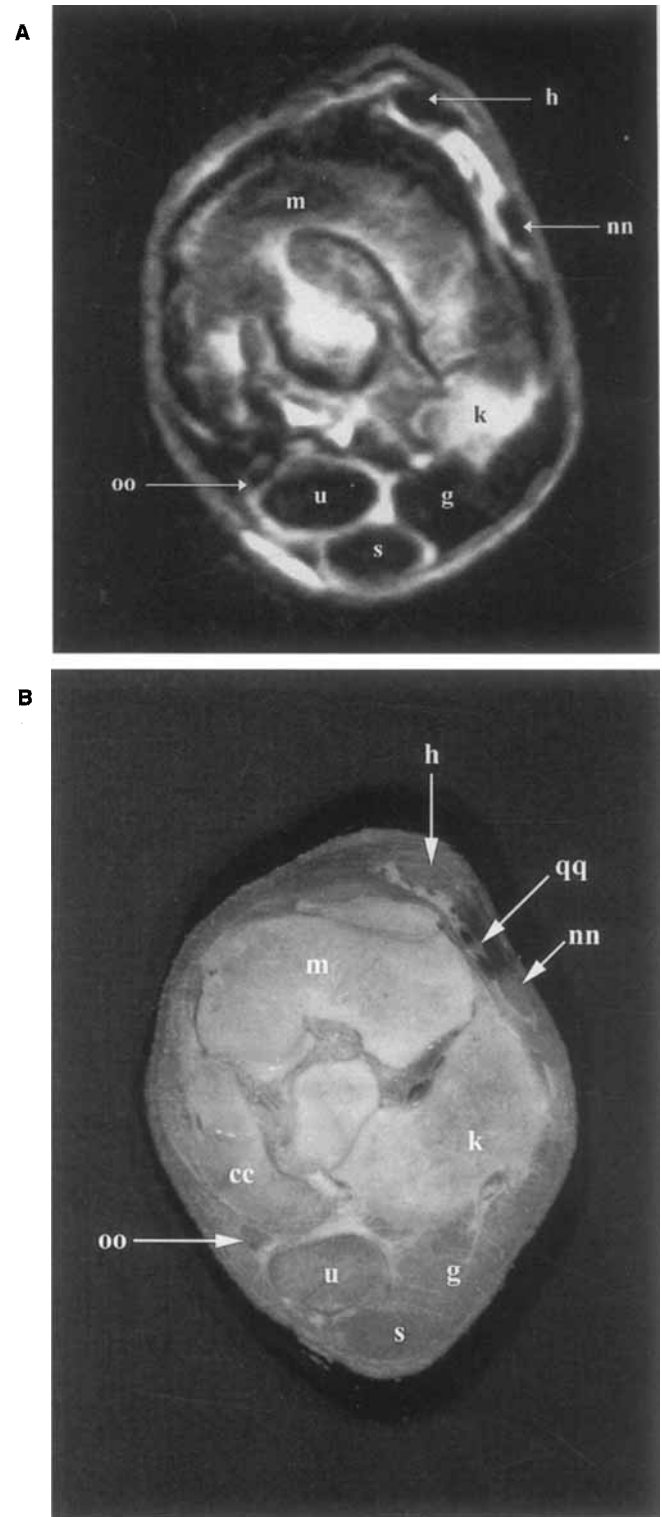


FIG. 9. (A) Transverse plane T1-weighted MR image and (B) gross anatomic section at the level of the distal row of tarsal bones. g) long plantar ligament; h) tendon of head of long digital extensor; k) fourth tarsal bone; m) third tarsal bone; s) tendon of superficial digital flexor; u) tendon of deep digital flexor; cc) fused first and second tarsal bones; nn) tendon of lateral digital extensor; oo) tendon of medial head of deep digital flexor; qq) deep peroneal nerve and cranial tibial vessels.

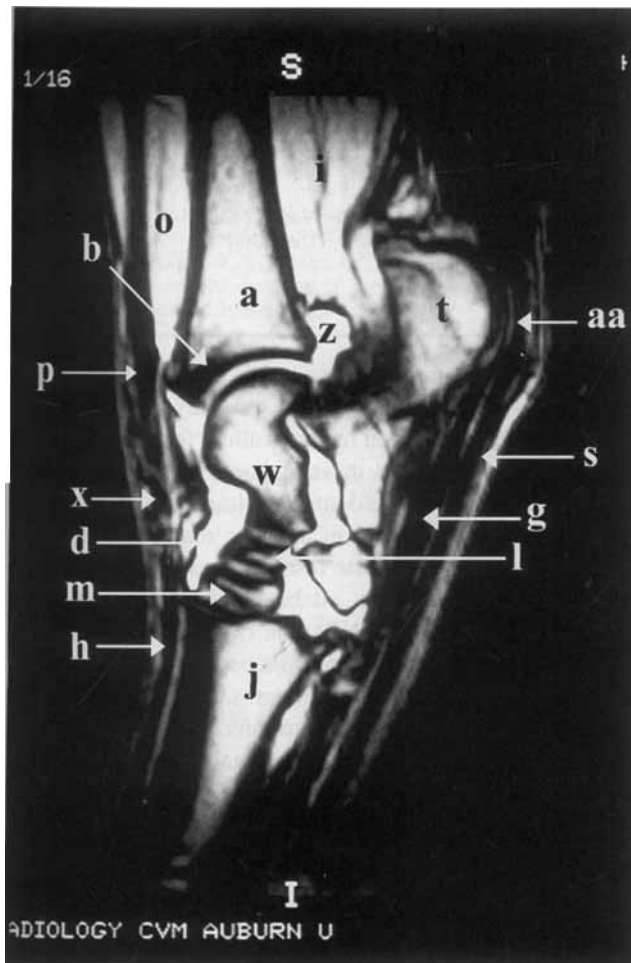


FIG. 10. Mid-sagittal plane T2-weighted MR image. a) marrow of tibia; d) synovium of tarsocrural joint; g) long plantar ligament; h) tendon of the long digital extensor; i) deep digital flexor muscle; j) metatarsal III; o) tibialis cranialis muscle; p) tendon of the peroneus tertius muscle; s) tendon of the superficial digital flexor; t) tuber calcanei; w) talus; x) medial tendon of tibialis cranialis muscle (cunean tendon); z) tarsocrural synovium; aa) calcaneal bursa.

tendon sheaths. Articular cartilage was well visualized on the T1-weighted images as a single homogenous layer of high to intermediate signal intensity immediately adjacent to a black layer of low signal intensity subchondral bone (Fig. 12). However, a single plane was not adequate for complete evaluation of the articular cartilage of the trochlear ridges of the talus. Signal volume averaging of these curved surfaces may have contributed to this finding.⁹ Thinner sections through the area may have reduced this effect but would have also reduced the signal resulting in lower resolution.¹² Fat and bone marrow had high signal intensity on T1-weighted images because of their large number of highly mobile hydrogen protons, which is consistent with previous reports.⁹⁻¹¹

The T2-weighted images were most useful for evaluating the synovium. It had very high signal intensity and appeared bright white on these images. Like the T1-weighted images,

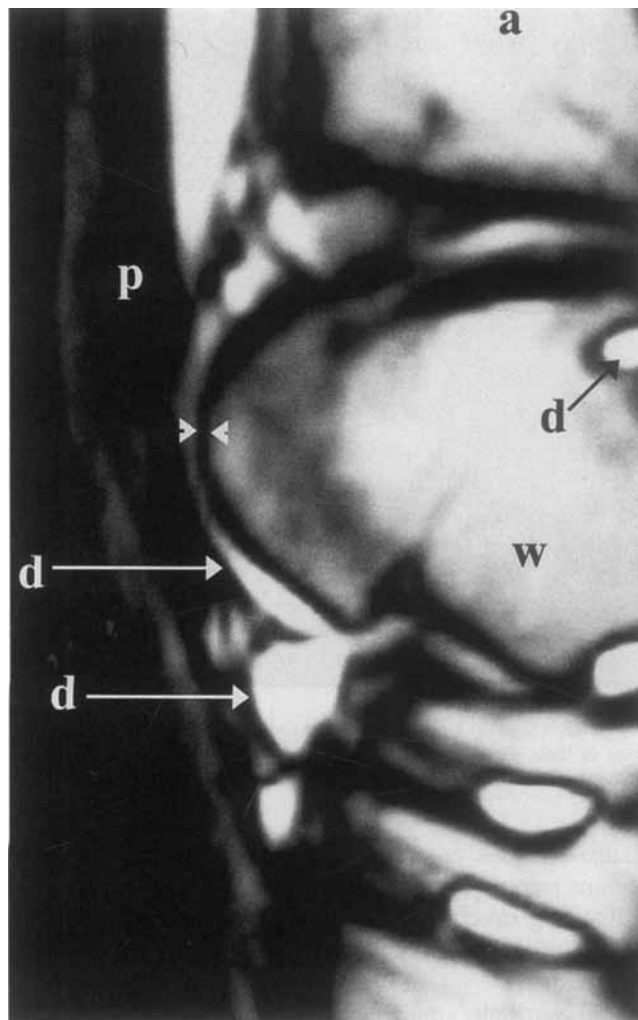


FIG. 11. Close up of Fig. 10. a) marrow of tibia; b) subchondral bone of tibia; d) synovium of tarsocrural joint; p) tendon of the peroneus tertius muscle; w) talus. Articular cartilage of the tarsocrural joint between arrowheads.

T2-weighted images had excellent definition of periarticular tendinous and ligamentous structures but T2-weighted images also provided excellent visualization of tendon sheaths and other synovial structures. However, T2-weighted images had less resolution than the T1-weighted images because of their lower SNR. Although the reduced resolution made T2-weighted images less than optimal for studying anatomic structures, they may prove to be very useful in recognition of disease processes. In T2-weighted images, greater signal production comes from tissues with longer T2 relaxation times. Consequently, T2 relaxation time of many abnormal tissues is longer because of more mobile hydrogen protons associated with an increase in tissue water content (i.e., edema, inflammation).⁴

Each of the three imaging planes contributed useful information concerning bony and soft tissue structures of the tarsus. However, certain anatomic structures were better vi-

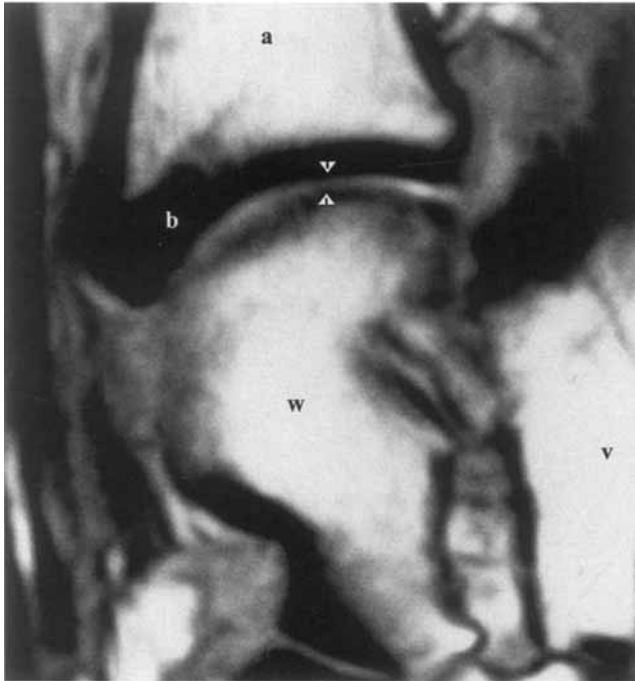


FIG. 12. Close up view of Fig. 3A. a) marrow of tibia; b) subchondral bone of tibia; v) sustentaculum tali; w) talus. Articular cartilage of tarsocrural joint between arrowheads.

sualized in one or more planes. Additionally, the use of oblique reconstruction techniques may have been useful for delineating structures, especially small tarsal bones where images often contained slices through both distal rows of bones.

Cadaver limbs are commonly used for evaluation of MR anatomy. Signal intensities seen in this study are very similar to those previously reported studies using cadaver limbs.² The primary difference between live and cadaver limbs is the signal intensity from vessels. Vascular structures in this study appeared as high signal intensity which is different from that recorded in live animals. Blood flow within vessels normally prevents good signal acquisition, and therefore, vascular structures of live animals are seen as areas of low signal intensity.¹³ The remainder of signal intensities generated from other tissues in this study should be similar to *in vivo* imaging. If differences in T1 or T2 relaxation times existed, they should not have affected image quality enough to alter appreciation of anatomic structures.

TABLE 2. Appearance of Normal Tissues on T1 and T2-Weighted Low-Field Magnetic Resonance Images

Tissue	T1	T2
Trabecular Bone	White	Gray
Subchondral/Cortical Bone	Black	Black
Articular Cartilage	Light Gray	Dark Gray to Black
Muscle	Variable Gray	Gray
Tendon/Ligaments	Dark Gray to Black	Dark Gray
Fat	White	Gray
Synovium	Gray	White

Magnet configuration (open versus tunnel designed gantries) limits the size of the patient and body part of the horse that can be imaged. Open magnets allow for the scanning of larger patients; however, these magnets are usually of lower field strength. Lower field strength implies a lower signal-to-noise ratio that results in a lower resolution or longer imaging times for the same resolution as a higher strength magnet.¹⁴ Image quality is a debatable issue, because image contrast-to-noise ratio (CNR), the ratio of image intensity difference between two tissues and background noise, tends to be higher at lower field strengths.¹¹ It is generally believed that image quality is determined by SNR; however, CNR may be a more clinically relevant parameter for distinguishing one tissue type from another (i.e., general lesion detectability).¹⁴ Low-field magnets offer the additional advantage of a lower fringe field that can accommodate anesthetic equipment within the scanning room.¹¹ Economically, low-field magnets have lower start-up and operating costs, require less siting room, and do not need cryogenics.¹¹ In addition, it is probable that portable magnets will be designed for use in the equine industry. Inevitably, these magnets will be of low field strength. All of these factors make low-field magnets attractive to the veterinary profession; therefore, it is important that the normal low-field MRI appearance of various equine anatomic structures be recognized.

The findings of this study indicate that low-field MRI can be used to identify the anatomic components of the equine tarsus and has the potential to become a useful imaging tool for equine orthopedic disease. Low-field MRI could be used to diagnose and study conditions such as osteoarthritis, osteochondrosis, tendinitis and desmitis, and intraarticular fractures involving tarsal joints. Additional studies utilizing low-field MRI in the evaluation of these pathologic conditions are needed.

REFERENCES

- Rose RJ, Hodgson DR. Hindlimb Abnormalities. In Rose and Hodgson. Manual of Equine Practice. Philadelphia: W.B. Saunders, 1993:112.
- Matrinelli MJ, Baker GJ, Clarkson RB, Eurell JC, Pijanowski GJ, Kuriashkin IV. Magnetic resonance imaging of degenerative joint disease in a horse: a comparison to other diagnostic techniques. *Equine Vet J* 1996;28:410-415.
- Crass JR, Genovese RL, Render JA, Bellon EM. Magnetic resonance, ultrasound and histopathologic correlation of acute and healing equine tendon injuries. *Vet Radiol & Ultrasound* 1992;33:210-216.
- Peterfy CG, Linares R, Steinbach LS. Recent advances in magnetic resonance imaging of the musculoskeletal system. *Radiologic Clinics of North America* 1994;32:291-311.

5. Nickel R, Schummer A, Seiferle E, Frewin J, Wille KH. The anatomy of the domestic animals Vol 1, The locomotor system of the domestic mammals. New York: Springer-Verlag, 1986.
6. Getty R. Equine osteology. In: Getty R. Sisson and Grossman's The anatomy of the domestic animals, 5th ed. Philadelphia: WB Saunders, 1975.
7. Sisson S. Equine syndesmology. In: Getty R. Sisson and Grossman's The anatomy of the domestic animals, 5th ed. Philadelphia: WB Saunders, 1975.
8. Sisson S. Equine myology. In: Getty R. Sisson and Grossman's The anatomy of the domestic animals, 5th ed. Philadelphia: WB Saunders, 1975.
9. Baird DK, Hathcock JT, Rumph PF, Kincaid SA, Visco DM. Low-field magnetic resonance imaging of the canine stifle joint: normal anatomy. *Vet Radiol & Ultrasound* 1998;39:87-97.
10. Rothschild PA, Domesek JM, Kaufman L et al. MR imaging of the knee with a 0.064-T permanent magnet. *Radiology* 1990;175:775-778.
11. Rothschild PA, Winkler ML, Gronemeyer DHW, Kaufman L, D'Amour P. Midfield and low-field magnetic resonance imaging of the spine. *Top Magn Reson Imag* 1988;1:11-23.
12. Kramer DM, Guzman RJ, Carlson JW, Crooks LE, Kaufman L. Physics of thin-section MR imaging at low field strength. *Radiology* 1989;173:541-544.
13. Chakers DW, Schmalbrock P. Magnetic resonance imaging of motion and flow. In: Chakers DW, Schmalbrock P. *Fundamentals of magnetic resonance imaging*. Baltimore: Williams and Wilkins, 1992.
14. Rutt, BK, Lee DH. The impact of field strength on image quality in MRI. *JMRI* 1996; 1:57-62.